Valence electronic charge density of distorted C_{60}^- monomers in polymerized KC_{60} and RbC_{60}

B. Verberck and V. N. Popov[a)]
Department of Physics, University of Antwerp, Universiteitsplein 1, 2610 Antwerp, Belgium

A. V. Nikolaev
Department of Physics, University of Antwerp, Universiteitsplein 1, 2610 Antwerp, Belgium and Institute of Physical Chemistry of the Russian Academy of Sciences, Leninskii Prospekt 31, 117915 Moscow, Russia

D. Lamoen
Department of Physics, University of Antwerp, Universiteitsplein 1, 2610 Antwerp, Belgium

(Received 3 March 2004; accepted 5 April 2004)

We investigate the valence electronic charge density of the C_{60}^- monomers in $(C_{60}^-)_n$ polymer chains in K- and RbC_{60} by means of a nonorthogonal tight-binding formalism using experimental data on the positions of the carbon atoms. Various configurations of the C_{60} cages are considered. Starting from the ideal icosahedral C_{60} structure and moving to the realistic, experimentally determined spatial configuration of the C_{60} cages in K- and RbC_{60}, we observe a systematic increase of the electric quadrupole moments on the C_{60}^- monomers. We also confirm the validity of factorizing the charge density of a C_{60}^- monomer into an angular and a radial part. © *2004 American Institute of Physics.* [DOI: 10.1063/1.1755676]

I. INTRODUCTION

The alkali metal doped C_{60} fullerides, A_xC_{60}, A=K, Rb, Cs, display a rich variety of interesting physical and chemical properties. For an overview, see Refs. 1–3. In particular, the $x=1$ compounds[4] have been found to form stable crystalline phases with cubic rocksalt structure (space group $Fm\bar{3}m$) at high temperature ($T \geqslant 350$ K) and polymeric phases[5–9] at lower temperatures.

The formation of polymers below 350 K explains the unusually short interfullerene distance—about 9% shorter than the usual 10 Å observed in molecular crystals containing C_{60} at ambient pressure—along the former cubic [110] direction. The linkage between neighboring C_{60} molecules is realized via covalent bonding between carbon atoms, the covalent bonds being formed through [2+2] cycloaddition reactions (Fig. 1), a scenario originally proposed to explain the creation of polymer chains in C_{60} fullerite (solid C_{60}) upon irradiating with photons—photopolymerization.[10] By now, an interfullerene distance of $d \approx 9.14$ Å has become a signature of covalent bonding, and various 1D and 2D fullerene polymers have been observed in C_{60} fullerite under high temperature–high pressure conditions.[11–17] The fullerene polymer chains in the AC_{60} alkali metal fullerides however are unique, not only because their reversible formation is thermally driven, but also because they accomodate one extra electron per C_{60} monomer since there is charge transfer of one electron from an alkali metal atom to a C_{60} molecule. Therefore, a C_{60} polymer chain in AC_{60} can be considered as a 1D chain with a valence electronic density having total charge $-e$ on every lattice site, but with a much more complex electronic structure than that of a simple atomic linear chain.

The goal of this paper is to study the valence electronic density of a $(C_{60}^-)_n$ polymer chain, taking into account the precise structure of the chain, i.e., using the experimentally measured positions of its constituting carbon atoms. The determination of the coordinates of the carbon atoms, together with the investigation of the AC_{60} crystallographic structure, has been carried out with increasing refinement over the years. From x-ray powder diffraction data, Stephens *et al.*[7] concluded that the polymer phase of both KC_{60} and RbC_{60} is orthorhombic with space group $Pmnn$ [Fig. 2(a)]. The direction of polymerization is the orthorhombic **b** axis (the former cubic [110] direction); the orientation of a polymer chain can be described by the angle ψ of the cycloaddition plane {the plane containing the carbon atoms C_1 participating in the [2+2] cycloaddition reactions [see Fig. 1(a)]} with the orthorhombic **c** axis (the former cubic [001] direction). In the $Pmnn$ structure, polymers have alternating orientations $\pm\psi$ in successive (**a**,**b**) planes. Since a chain of covalently bond undistorted C_{60} molecules would imply a too long interfullerene C_1-C_1 bond length of 2.23 Å, the positions of the C_1, C_2, and C_3 atoms [see Fig. 1(a)] were relaxed,[7] yielding more reasonable interfullerene C_1-C_1 distances of 1.44 Å (RbC_{60}) and 1.65 Å (KC_{60}). The C_1-C_1 interfullerene distance for RbC_{60} is comparable to the interatomic distance in an undistorted C_{60} molecule (≈ 1.40 Å), but implies a serious distortion of the C_{60} cage, with intermolecular C–C bond lengths ranging from 1.32 Å up to 1.9 Å. For RbC_{60}, a structure with a less distorted C_{60} cage but a larger interfullerene C_1-C_1 bond length (1.57 Å) was inferred from powder neutron diffraction measurements by Fox *et al.*[18] A

[a)]Permanent address: Faculty of Physics, University of Sofia, 5 J. Bourchier Boulevard, 1164 Sofia, Bulgaria.

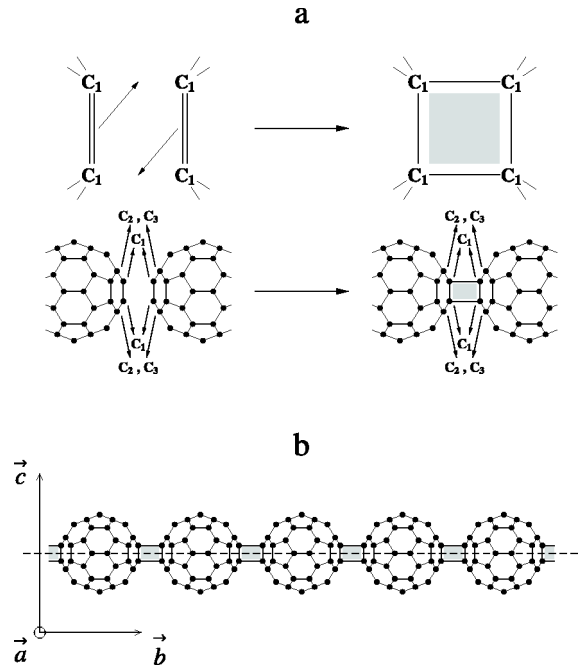

FIG. 1. (a) Below 350 K, polymer chains are formed in K-, Rb-, and CsC_{60} via [2+2] cycloaddition reactions: two opposing double carbon bonds "break" to form a cyclobutane fragment. The carbon atoms participating in the cycloaddition reaction, labeled C_1, lie in the (**b**,**c**) plane, while C_2 and C_3 lie above and below the (**b**,**c**) plane, respectively. (b) All cyclobutane fragments (shaded) of a polymer chain lie in a same plane, the cycloaddition plane, which characterizes the orientation of the chain in the crystal lattice. The polymer chain, which can rotate about its long axis (dashed), is said to be in the standard orientation when its cycloaddition plane is parallel to the crystallographic (**b**,**c**) plane.

powder neutron scattering study on KC_{60} performed by Guerrero *et al.*[19] also lead to a revised structure, with an interfullerence C_1-C_1 distance of 1.54 Å and again a less distorted C_{60} cage. Meanwhile, the crystal structure of both K- and RbC_{60} was reexamined by Launois *et al.*[8] by means of single crystal x-ray diffraction. While the orthorhombic space group $Pmnn$ was confirmed for KC_{60}, RbC_{60} was found to have a monoclinic Bravais lattice with space group $I2/m$, the monoclinic angle being very close to 90°, however. In the space group $I2/m$, all polymer chains have the same orientation [Fig. 2(b)]. It has been shown by Rouzière *et al.*[9] that CsC_{60} also has the $I2/m$ structure. The findings of Launois *et al.*[8] were confirmed by the detailed neutron powder diffraction study of Huq *et al.*,[20] who not only verified the space groups but also presented the atomic coordinates of the C_{60} cage for both K- and RbC_{60}. The interfullerene C_1-C_1 bond lengths were reported to be 1.6 Å and 1.55 Å for K- and RbC_{60}, respectively.

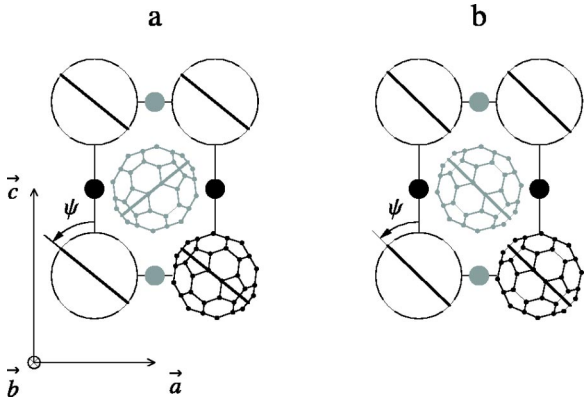

FIG. 2. Projections of the crystal structures of polymerized KC_{60} (a) and Rb-, CsC_{60} (b) onto the (**a**,**c**) crystallographic plane. The cycloaddition planes, perpendicular to the (**a**,**c**) plane, are marked by thick bars. The bigger dots represent the alkali metal atoms. The C_{60} monomers and the alkali metal atoms shown in black display a shift of $b/2$ along the **b** direction with respect to those shown in gray. In KC_{60} (space group $Pmnn$), the orientations of the polymer chains alternate along the **c** axis, while in Rb- and CsC_{60} (space group $I2/m$), all chains have the same orientation.

Now that both the crystal structure and the coordinates of the carbon atoms of K- and RbC_{60} are well established, it is possible to examine the electronic density distribution of the $(C_{60}^-)_n$ polymer chains in more detail and estimate their electric quadrupole components. It was shown that the electric quadrupole on a C_{60}^- monomer plays a crucial role in explaining the different crystallographic space groups of the AC_{60} compounds.[21,22] In particular, it was demonstrated that the alkali metal mediated interaction between neighboring C_{60}^- quadrupoles is the decisive mechanism yielding the $Pmnn$ structure for KC_{60} and the $I2/m$ structure for Rb- and CsC_{60}. However, the two aforementioned theoretical works addressing the problem of the crystal structures of the AC_{60} polymer phases employ a simple dumbbell-like model of point charges to describe the electric quadrupole on a C_{60}^- monomer. A more realistic charge distribution as the result of a simplified Slater–Koster tight-binding approach was presented in Ref. 23. There, the three t_{1u} molecular orbitals, forming an irreducible representation of the icosahedral group I_h, were used to describe the extra electron on a C_{60}^- monomer, while the cycloaddition bonds were modeled by a potential consisting of contact interactions representing the orthorhombic (D_{2h}) symmetry of a polymer chain. In this work, we abandon the approximation of having C_{60}^- monomers with icosahedral (I_h) symmetry and use the coordinates of the distorted C_{60}^- units as input for tight-binding calculations. We show that the distortion of the C_{60} cage enhances the quadrupole moment of its charge distribution significantly, and we make a comparison between KC_{60} and RbC_{60}, the former exhibiting a higher degree of distortion than the latter.[20] Our numerical values are relevant for a quantum mechanical description of the alkali metal specific quadrupolar interactions in the AC_{60} solids,[24] responsible for the different crystal structures of polymerized KC_{60} and Rb-, CsC_{60}.[21,22]

II. STEPWISE APPROACH

In order to achieve a thorough understanding of the formation of electric quadrupoles on the C_{60}^- monomers, we proceed in several steps. First, we consider isolated C_{60} molecules (having I_h symmetry) linked together forming a chain of undeformed neutral C_{60} monomers. Next, we charge every C_{60} monomer with one electron. Then, we take into account the deformation of the C_{60} units. As described in the Introduction, the experimental efforts to determine the structure of the C_{60} cages have culminated in the neutron powder scat-

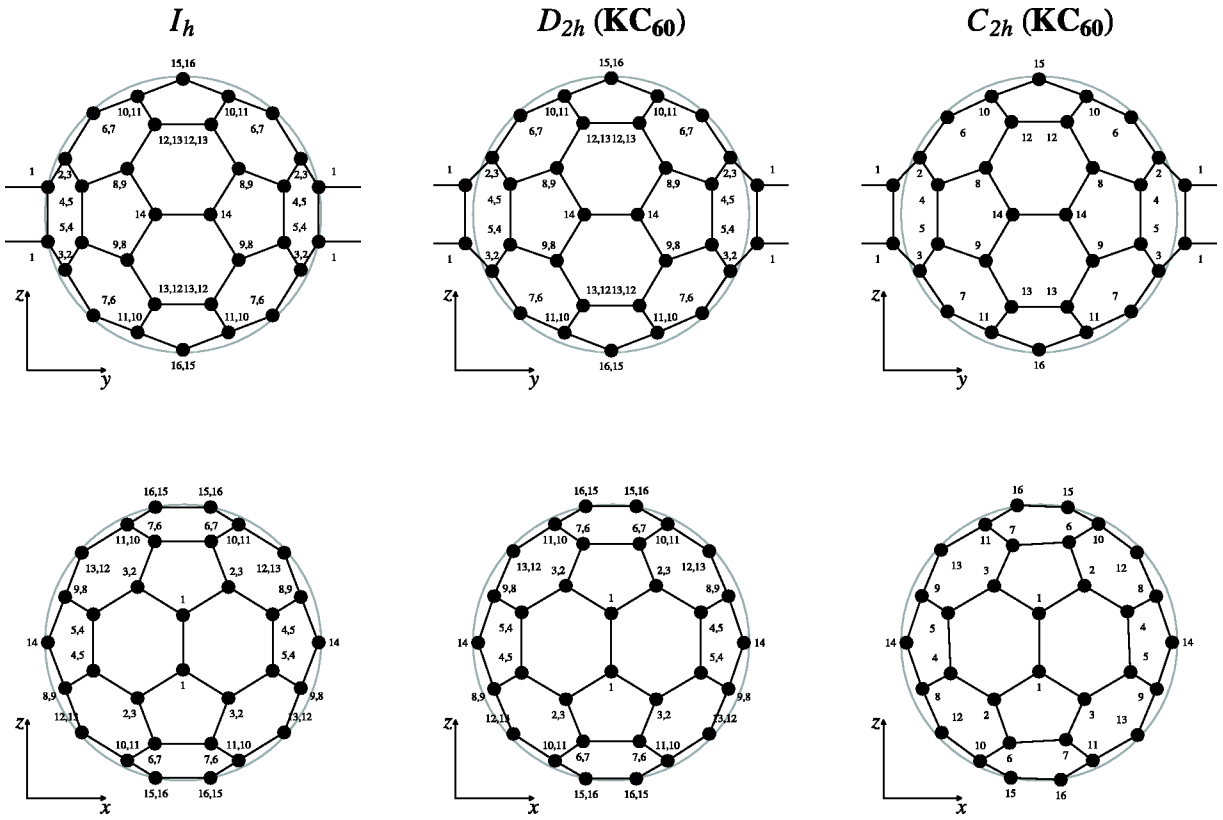

FIG. 3. The C_{60} cage, projected onto the (**b**,**c**) plane (top row) and the (**a**,**c**) plane (bottom row) for different configurations: icosahedral (left), D_{2h} (middle), and C_{2h} (right). For the icosahedral (I_h) case, the C_{60} cage coincides with a regular truncated icosahedron. The shown C_{2h} configuration (right) is that of KC_{60} at $T=300$ K (the coordinates have been taken from Ref. 20). Note that the cycloaddition plane is not a mirror plane. From the C_{2h} structure, we have constructed a D_{2h} unit (middle) by averaging the C_{2h} coordinates. The numeration of carbon atoms of Ref. 20 has been followed; pairwise notation indicates equivalence. In the C_{2h} projection onto the (**b**,**c**) plane (top right), one hemisphere has been omitted for clarity. In all other cases the projections of the two hemispheres coincide. The shown circle with radius $R_{C_{60}}$ allows a visual estimation of the nonideality of the C_{60} cage in the C_{2h} and D_{2h} configurations. The elongation of the monomer along the polymerization direction (y axis) can be clearly seen.

tering study of Huq *et al.*,[20] reaching a very high degree of precision. There it was found that the C_{60} balls are deformed in such a way that they have C_{2h} symmetry. The symmetry not being icosahedral (I_h) does not come as a surprise of course, but for KC_{60} one would intuitively expect orthorhombic (D_{2h}) symmetry—the symmetry of the crystal lattice. The symmetry being C_{2h} and not D_{2h} implies that the cycloaddition plane [see Fig. 1(b)] is no longer a mirror plane; the polymerization axis (parallel to the **b** axis) remains a twofold axis though, as illustrated for KC_{60} in the right part of Fig. 3. Also, the axis perpendicular to the cycloaddition plane and running through the center of the monomer is no longer a twofold axis.

Within our view, the polymer chains not having D_{2h} symmetry is a consequence of their ''settling'' in a final orientational configuration [$\psi_{KC_{60}}=\pm 50°$, see Fig. 2(a)]. Therefore, we think it useful to consider D_{2h} distorted C_{60} balls as well. For RbC_{60}, the C_{2h} symmetry is compatible with the monoclinic crystal structure [Fig. 2(b)], but since the monoclinic angle is extremely close to 90° [$\alpha=90.316°$ (Ref. 20)], we also present D_{2h} symmetry calculations for RbC_{60}, as if the crystal lattice were orthorhombic (an approximation used in other theoretical works[21,22,25]). We have constructed the D_{2h} C_{60} units by mirroring the C_{2h} structure about the cycloaddition plane, then rotating it over π along the axis parallel to **a** and running through the center of the monomer, and finally averaging the coordinates of the so-generated coordinates so that the originally inequivalent carbon atoms (e.g., atoms 2 and 3 in Fig. 3) end up having the desired equivalencies of atoms, yielding D_{2h} symmetry for the C_{60} cage. The middle part of Fig. 3 visualizes the D_{2h} unit for KC_{60}. Upon comparing the right (C_{2h}) and middle (D_{2h}) parts of Fig. 3 to the left (I_h) part, it is clearly seen that the main distortional feature is the displacement of the carbon atoms participating in the cycloaddition bond (the atoms labeled 1), and that this is preserved when averaging the C_{2h} configuration to a D_{2h} one.

We refer to the various steps as follows: (a) uncharged, undistorted (I_h), isolated C_{60} molecule, (b) chain of undistorted (I_h) neutral C_{60} monomers, (c) chain of undistorted (I_h) charged C_{60}^- monomers, (d) chain of D_{2h} distorted C_{60}^- monomers, (e) chain of C_{2h} distorted C_{60}^- monomers. The last two cases are different for K- and RbC_{60} since they involve the actual positions of the carbon atoms. We recall that according to our opinion, the C_{2h} symmetry of the C_{60}^- monomer is the result of the fixed orientations of the polymer chains in the crystal. Hence, case (d) can be considered as the end point if one studies a single polymer chain, or a hypothetical $Immm$ phase, involving freely rotating or, alternatively, randomly oriented polymer chains.[22]

III. CHARGE DISTRIBUTION, QUADRUPOLE MOMENTS, RADIAL DISTRIBUTION

As a result of the charge transfer of one electron from an alkali metal atom to a C_{60} molecule, a charge distribution $\rho(r)$ with total charge $Q_0=\int d\mathbf{r}\rho(\mathbf{r})=-e$ exists on every C_{60} molecule.

In order to be able to make a comparison between the charge distributions of the different cases described in the previous section, we consider the multipole expansion of the electrostatic potential $\Phi(\mathbf{r})$ set up by the charge distribution $\rho(\mathbf{r})$,

$$\Phi(\mathbf{r})=\frac{1}{4\pi\epsilon_0}\left(\frac{Q_0}{r}+\frac{\mathbf{d}\cdot\mathbf{r}}{r^3}+\frac{1}{2}\sum_{i=1}^{3}\sum_{j=1}^{3}\frac{Q_{ij}x_ix_j}{r^5}+\cdots\right). \tag{3.1}$$

Here, $\mathbf{d}=\int d\mathbf{r}\mathbf{r}\rho(\mathbf{r})$ is the dipole moment and

$$Q_{ij}=\int d\mathbf{r}(3x_ix_j-\delta_{ij}r^2)\rho(\mathbf{r}) \tag{3.2}$$

are the quadrupole moments. The dipole moment vanishes for a charge distribution with C_{2h} (or D_{2h} or I_h) symmetry, so that the quadrupole terms of expansion (3.1) comprise the first nontrivial contributions to $\Phi(\mathbf{r})$,

$$\Phi(\mathbf{r})=\frac{1}{4\pi\epsilon_0}\left(\frac{Q_0}{r}+\frac{1}{2}\sum_{i=1}^{3}\sum_{j=1}^{3}\frac{Q_{ij}x_ix_j}{r^5}+\cdots\right). \tag{3.3}$$

The numerical calculation of the quadrupole moments Q_{ij} is carried out using a nonorthogonal tight-binding model with parameters taken from an *ab initio* study of carbon clusters.[26] The electronic eigenvalue problem is solved for 60 **k**-points of the one-dimensional Brillouin zone of the $(C_{60}^{-})_n$ chain. The wave functions are then constructed by means of the $2s$- and $2p$-type atomic orbitals of carbon and the expansion coefficients of the wave function. The obtained electron density $\rho(\mathbf{r})$ is used to calculate the quadrupole moments Q_{ij} via Eq. (3.2) by numerical integration over a $100\times100\times100$ points grid in a unit cell with a lateral size of 10 Å. The number of **k**-points and the integration grid insure accuracy of 0.01 atomic units for the quadrupole moments. The carbon atoms constituting the undistorted C_{60} cage are located at the corner points of a regular truncated icosahedron, circumscribed by a sphere of radius $R_{C_{60}}=3.55$ Å (Ref. 27) (Fig. 3, left). For the actual C_{2h} carbon coordinates (and the therefrom derived D_{2h} coordinates) in polymerized KC_{60} (Fig. 3, right) and RbC_{60}, we use the values provided by Huq *et al.*[20] obtained from Rietveld fits to measurements at $T=300$ K and $T=200$ K for KC_{60} and RbC_{60}, respectively.

To establish the link with the previous theoretical work[23] where a factorization of the charge distribution into a radial and an angular part (originating from a same factorization of the electronic wave function) was assumed,

$$\rho(\mathbf{r})=\rho(r,\theta,\phi)=-e\mathcal{R}(r)\mathcal{A}(\theta,\phi), \tag{3.4}$$

we consider the expansion of $\rho(\mathbf{r})$ in spherical harmonics,

$$\rho(\mathbf{r})=\sum_l\sum_\tau\rho_l^\tau(r)Y_l^\tau(\theta,\phi). \tag{3.5}$$

We use the real spherical harmonics of Ref. 28. Replacing $\mathcal{A}(\theta,\phi)$ in Eq. (3.4) by its expansion in spherical harmonics,

$$\mathcal{A}(\theta,\phi)=\sum_l\sum_\tau c_l^\tau Y_l^\tau(\theta,\phi), \tag{3.6}$$

and then comparing Eqs. (3.4) and (3.5), one gets

$$\rho_l^\tau(r)=-ec_l^\tau\mathcal{R}(r). \tag{3.7}$$

Using the definition of Q_{ij}, Eq. (3.2), and using the decomposition of $\rho(\mathbf{r})$ into spherical harmonics, Eqs. (3.5) and (3.7), one can derive the following relations between the Cartesian quadrupole moments Q_{ij} and the spherical quadrupole moments $c_{l=2}^\tau$,

$$c_2^0=\frac{1}{e\tilde{g}}\sqrt{\frac{5}{16\pi}}(Q_{11}+Q_{33}), \tag{3.8a}$$

$$c_2^{1,c}=\frac{1}{e\tilde{g}}\sqrt{\frac{5}{12\pi}}Q_{12}, \tag{3.8b}$$

$$c_2^{1,s}=\frac{1}{e\tilde{g}}\sqrt{\frac{5}{12\pi}}Q_{23}, \tag{3.8c}$$

$$c_2^{2,c}=-\frac{1}{e\tilde{g}}\sqrt{\frac{5}{48\pi}}(Q_{11}-Q_{33}), \tag{3.8d}$$

$$c_2^{2,s}=-\frac{1}{e\tilde{g}}\sqrt{\frac{5}{12\pi}}Q_{13}. \tag{3.8e}$$

For a D_{2h} or I_h charge distribution, the second order moments $c_2^{1,c}$, $c_2^{1,s}$, and $c_2^{2,s}$ are zero, because D_{2h} and I_h symmetries imply diagonality of the quadrupole tensor $[Q]$. Full details of the derivation are given in Appendix A. The parameter $\tilde{g}$ is related to the precise expression for the radial part $\mathcal{R}(r)$:

$$\tilde{g}=\int drr^4\mathcal{R}(r). \tag{3.9}$$

The radial part can be approximated with the simple expression

$$\mathcal{R}(r)=\frac{\delta(r-R)}{R^2}, \tag{3.10}$$

corresponding to a distribution of the charge on a spherical shell of radius R, and yielding a factor $\tilde{g}=R^2$. In Table I, the results of the calculations are presented for the various cases introduced in the preceding section; the conversion from Cartesian to spherical quadrupole moments has been done using radial part (3.10) with $R=R_{C_{60}}$.

As mentioned earlier, the conversion from Cartesian to spherical quadrupolar moments is introduced here for the purpose of comparison with the results of the earlier work.[23] However, it also allows better comparison of the ''overall'' magnitude of the electrical quadrupole of the cases under consideration in this work, since it is difficult to compare the quadrupole tensors $[Q]$ directly because of their tracelessness,

$$Q_{11}+Q_{22}+Q_{33}=0, \tag{3.11}$$

TABLE I. Cartesian quadrupole moments Q_{ij}, $i,j=1,2,3$, and spherical quadrupole moments c_2^0, $c_2^{1,c}$, $c_2^{1,s}$, $c_2^{2,c}$, and $c_2^{2,s}$ for the various C_{60} units described in Sec. II [cases (a)–(e)]. The spherical moments (dimensionless) are derived from the Cartesian moments (in atomic units $ea_0^2=4.4866\times10^{-40}$ C m^2, $-e$ being the electron charge and a_0 the Bohr radius) via Eqs. (3.8a)–(3.8e), with $\tilde{g}=R^2$ and $R=R_{C_{60}}$. The quadrupole tensor [Eq. (3.2)] is symmetric. Column (f) lists the spherical quadrupole moments of Ref. 23 and therefrom [via the inverse transformation of Eqs. (3.8a)–(3.8e)] calculated Cartesian quadrupole moments. Although cases (c) and (f) represent the same physical situation, different numerical values arise due to different tight-binding approaches.

	(a) Uncharged undistorted isolated	(b) Uncharged undistorted chain	(c) Charged undistorted chain	(d) Charged D_{2h} distorted chain		(e) Charged C_{2h} distorted chain		(f) Charged undistorted chain
				KC_{60}	RbC_{60}	KC_{60}	RbC_{60}	
Q_{11}	0	2.83	−4.58	−54.39	−63.25	−55.15	−59.30	3.46
Q_{22}	0	0.03	17.97	66.15	77.66	65.85	80.45	3.47
Q_{33}	0	−2.86	−13.40	−11.76	−14.41	−10.70	−21.15	−6.92
Q_{12}	0	0	0	0	0	0	0	0
Q_{13}	0	0	0	0	0	−16.36	−7.07	0
Q_{23}	0	0	0	0	0	0	0	0
c_2^0	0	0.000	−0.1259	−0.4636	−0.5442	−0.4615	−0.5638	−0.0243
$c_2^{1,c}$	0	0	0	0	0	0	0	0
$c_2^{1,s}$	0	0	0	0	0	0	0	0
$c_2^{2,c}$	0	−0.023	−0.0357	0.1725	0.1976	0.1798	0.1544	−0.0420
$c_2^{2,s}$	0	0	0	0	0	0.1324	0.0572	0

which makes the six moments Q_{ij} presented in Table I a linearly dependent set, whereas the set of five spherical quadrupole moments c_2^0, $c_2^{1,c}$, $c_2^{1,s}$, $c_2^{2,s}$, and $c_2^{2,s}$ are linearly independent. Nevertheless, one must keep in mind that the validity of the conversion from Q_{ij} to $c_{l=2}^{\tau}$ via Eqs. (3.8a)–(3.8e) relies entirely on the factorization assumption (3.4). Indeed, for C_{60}^- monomers lacking I_h symmetry, e.g., cases (d) and (e), ansatz (3.4) does not hold, and, as a consequence, the radial dependence of the coefficients ρ_l^{τ} will not a priori be simply a "universal" function $-e\mathcal{R}(r)$ times an (l,τ) dependent constant c_l^{τ} [Eq. (3.7)]. However, the spherical quadrupole moments do make sense as a first (spherical) approximation for a C_{60}^- unit. Indeed, in theoretical studies it is usually understood that such a factorization is valid if not reasonably approximate. Once assumption (3.4) is made, the radial part $\mathcal{R}(r)$ often turns out to be irrelevant, e.g., for properties related to the orientation of the C_{60} units.[25] Since we have the full charge distribution $\rho(\mathbf{r})$ at our disposal, we can test factorization ansatz (3.4) by numerically deriving the radial distribution $\mathcal{R}(r)$ from our values of $\rho(\mathbf{r})$. It is clear that this is basically nothing more than performing an average of $\rho(\mathbf{r})$ over the angular coordinates. The recipe is outlined in Appendix B. Figure 4 shows the results of our calculations of $\mathcal{R}(r_k)$ for values of r_k ranging from 0 to 4.5 Å in steps of approximately 0.045 Å, for the "charged" cases (c), (d), and (e), the latter two for both K- and RbC_{60}.

IV. DISCUSSION AND CONCLUSIONS

We now turn to a discussion of the results. As explained above, we prefer to focus on the spherical quadrupole components for making comparative statements. A first major conclusion that can be drawn from Table I is that upon introducing the linkage between neighboring C_{60} molecules, nonzero quadrupole moments appear, even for neutral C_{60} monomers [case (b)]. Upon charging the C_{60} units [case (c)], the magnitude of the quadrupole components increases. A further increase is observed when one compares any of the distorted cases [(d) and (e)] with the undistorted case (c). Therefore, as a second major conclusion, we can state that both charging and distorting the C_{60} monomers leads to a considerable increase of the quadrupole moments. This conclusion is particularly relevant for the mechanism of Refs. 21, 22, and 24 explaining the different crystal structures of K- and Rb-, CsC_{60}, where the quadrupolar polarizability of the alkali ions—induced by the electric quadrupoles on the C_{60}^- monomers—plays a key role. Comparing the results of KC_{60} and RbC_{60}, we observe that, although the C_{60} unit is more distorted in KC_{60} than in RbC_{60},[20] the values of the quadrupole moments lie close to each other (excepting $c_2^{2,s}$, which is roughly a factor of 2 larger for K- than for RbC_{60}).

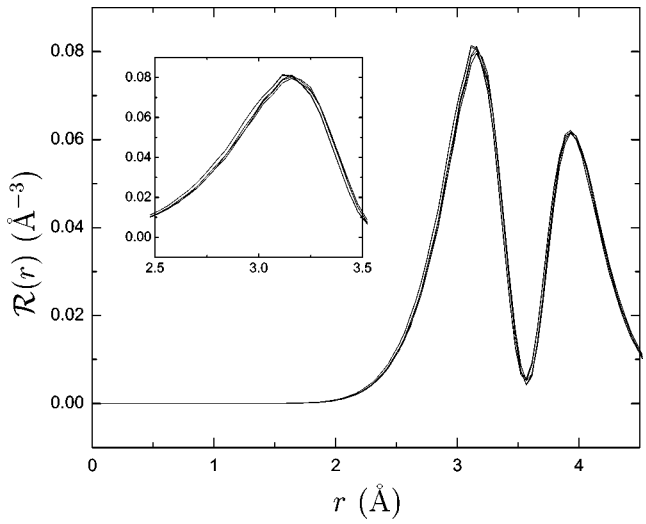

FIG. 4. Radial part $\mathcal{R}(r)$ of the valence charge density $\rho(\mathbf{r})=\rho(r,\theta,\phi)$ of a C_{60}^- monomer, obtained by averaging over θ and ϕ. All five charged cases are presented (I_h, D_{2h}–KC_{60}, D_{2h}–RbC_{60}, C_{2h}–KC_{60}, and C_{2h}–RbC_{60}); the five curves nearly coincide (inset). The normalization condition reads $4\pi\int_0^{\infty}r^2dr\mathcal{R}(r)=1$ (see Appendix B).

Also, apart from the appearance of $c_2^{2,s}$, there is no substantial difference between the D_{2h} and C_{2h} situations (making the D_{2h} C_{60} cage a justified approximation).

As for our calculations of the radial distributions (Fig. 4), it can be clearly seen that the five $\mathcal{R}(r)$ curves lie extremely close to each other. The important conclusion one can draw from this is that not only the factorization ansatz must hold fairly well, but also that the radial part $\mathcal{R}(r)$ hardly changes upon distorting the C_{60}^- monomers (reducing the symmetry from I_h to D_{2h} or even C_{2h}). The two-peak shape of $\mathcal{R}(r)$ with a minimum at $R_{C_{60}}=3.55$ Å is reminiscent of one of the radial models presented in Ref. 29 (model III, dotted line in Fig. 4 therein), which is thus by the present calculations proven to be an applicable approximation.

In summary, our main conclusions concerning the electric quadrupole moments of a $(C_{60}^-)_n$ polymer chain are that (i) linking the C_{60} molecules into a chain, (ii) charging, and (iii) deforming them so that they have D_{2h} (or C_{2h}) symmetry all increase the quadrupole moments of their valence charge density. Finally, we also have shown that factorizing the valence charge density of a C_{60}^- monomer in a $(C_{60}^-)_n$ polymer chain into an angular and a radial part makes a valid approximation.

ACKNOWLEDGMENTS

The authors wish to thank K.H. Michel for suggesting this problem and for constructive discussions. B.V. is a research assistant of the Fonds voor Wetenschappelijk Onderzoek – Vlaanderen. V.N.P. acknowledges financial support from the Bijzonder Onderzoeksfonds, Universiteit Antwerpen (BOF). A.V.N. acknowledges financial support from the Bijzonder Onderzoeksfonds, Universiteit Antwerpen (BOF-NOI).

APPENDIX A: FROM CARTESIAN TO SPHERICAL QUADRUPOLE MOMENTS

The Cartesian coordinate system (x,y,z) we use is that of Ref. 20, i.e., $x\leftrightarrow\mathbf{a}$, $y\leftrightarrow\mathbf{b}$, $z\leftrightarrow\mathbf{c}$, with $\mathbf{b}$ the direction of polymerization, and the plane of cycloaddition coinciding with the ($\mathbf{b}$,$\mathbf{c}$) plane [standard orientation, Fig. 1(b)]. The spherical coordinate system (r',θ',ϕ') employed is that of Ref. 23 however, so that care must be taken when formulating the proper coordinate transformation. It reads

$$x=x'=r'\sin\theta'\cos\phi', \tag{A1a}$$

$$z=y'=r'\sin\theta'\sin\phi', \tag{A1b}$$

$$-y=z'=r'\cos\theta', \tag{A1c}$$

where the auxiliary Cartesian coordinates (x',y',z') display the usual relation to (r',θ',ϕ'). For notational simplicity, we drop the primes of (r',θ',ϕ') and write

$$\frac{x}{r}=\sin\theta\cos\phi, \tag{A2a}$$

$$\frac{z}{r}=\sin\theta\sin\phi, \tag{A2b}$$

$$-\frac{y}{r}=\cos\theta. \tag{A2c}$$

The real spherical harmonics $Y_{l=2}^{\tau}\equiv Y_{l=2}^{\tau}(\theta,\phi)$ of Ref. 28 can then be expressed as functions of the Cartesian coordinates,

$$Y_2^{0,c}=\sqrt{\frac{5}{16\pi}}(3\cos^2\theta-1)=\sqrt{\frac{5}{16\pi}}\frac{3y^2-r^2}{r^2}, \tag{A3a}$$

$$Y_2^{1,c}=\sqrt{\frac{15}{4\pi}}\sin\theta\cos\theta\cos\phi=-\sqrt{\frac{15}{4\pi}}\frac{xy}{r^2}, \tag{A3b}$$

$$Y_2^{1,s}=\sqrt{\frac{15}{4\pi}}\sin\theta\cos\theta\sin\phi=-\sqrt{\frac{15}{4\pi}}\frac{yz}{r^2}, \tag{A3c}$$

$$Y_2^{2,c}=\sqrt{\frac{15}{16\pi}}\sin^2\theta(\cos^2\phi-\sin^2\phi)=\sqrt{\frac{15}{16\pi}}\frac{x^2-z^2}{r^2}, \tag{A3d}$$

$$Y_2^{2,s}=2\sqrt{\frac{15}{16\pi}}\sin^2\theta\sin\phi\cos\phi=2\sqrt{\frac{15}{16\pi}}\frac{xz}{r^2}. \tag{A3e}$$

Next, the quantities $\tilde{Q}_{ij}\equiv\tilde{Q}_{ij}(\mathbf{r})=3x_ix_j-\delta_{ij}r^2$ appearing in the expression for the Cartesian quadrupole moments Q_{ij} [Eq. (3.2)] can be written in terms of the functions (A3a)–(A3e),

$$\tilde{Q}_{11}=3x^2-r^2=\sqrt{\frac{16\pi}{5}}\left(-\frac{1}{2}Y_2^{0,c}+\frac{\sqrt{3}}{2}Y_2^{2,c}\right)r^2, \tag{A4a}$$

$$\tilde{Q}_{22}=3y^2-r^2=\sqrt{\frac{16\pi}{5}}Y_2^{0,c}r^2, \tag{A4b}$$

$$\tilde{Q}_{33}=3z^2-r^2=\sqrt{\frac{16\pi}{5}}\left(-\frac{1}{2}Y_2^{0,c}-\frac{\sqrt{3}}{2}Y_2^{2,c}\right)r^2, \tag{A4c}$$

$$\tilde{Q}_{12}=3xy=-3\sqrt{\frac{4\pi}{15}}Y_2^{1,c}r^2, \tag{A4d}$$

$$\tilde{Q}_{13}=3xz=\frac{3}{2}\sqrt{\frac{16\pi}{15}}Y_2^{2,s}r^2, \tag{A4e}$$

$$\tilde{Q}_{23}=3yz=-3\sqrt{\frac{4\pi}{15}}Y_2^{1,s}r^2. \tag{A4f}$$

Finally, by performing the integration of $\tilde{Q}_{ij}(\mathbf{r})\rho(\mathbf{r})$ over all space in spherical coordinates,

$$Q_{ij}=\int_0^\infty r^2dr\int_0^\pi\sin\theta d\theta\int_0^{2\pi}d\phi\tilde{Q}_{ij}(r,\theta,\phi)\rho(r,\theta,\phi), \tag{A5a}$$

using

$$\rho(r,\theta,\phi)=-e\mathcal{R}(r)\sum_{l'}\sum_{\tau'}c_{l'}^{\tau'}Y_{l'}^{\tau'}(\theta,\phi) \tag{A5b}$$

and the orthogonality relation

$$\int_0^\pi\sin\theta\int_0^{2\pi}d\phi Y_{l=2}^{\tau}Y_{l'}^{\tau'}=\delta_{l=2,l'}\delta_{\tau,\tau'}, \tag{A5c}$$

one gets the following linear system of equations relating Q_{ij} to $c_{l=2}^{\tau}$:

$$Q_{11}=-e\tilde{g}\sqrt{\frac{16\pi}{5}}\left(-\frac{1}{2}c_2^{0,c}+\frac{\sqrt{3}}{2}c_2^{2,c}\right), \tag{A6a}$$

$$Q_{22}=-e\tilde{g}\sqrt{\frac{16\pi}{5}}c_2^{0,c}, \tag{A6b}$$

$$Q_{33}=-e\tilde{g}\sqrt{\frac{16\pi}{5}}\left(-\frac{1}{2}c_2^{0,c}-\frac{\sqrt{3}}{2}c_2^{2,c}\right), \tag{A6c}$$

$$Q_{12}=3e\tilde{g}\sqrt{\frac{4\pi}{15}}c_2^{1,c}, \tag{A6d}$$

$$Q_{13}=-\frac{3}{2}e\tilde{g}\sqrt{\frac{16\pi}{15}}c_2^{2,s}, \tag{A6e}$$

$$Q_{23}=3e\tilde{g}\sqrt{\frac{4\pi}{15}}c_2^{1,s}, \tag{A6f}$$

where $\tilde{g}=\int_0^\infty drr^4\mathcal{R}^2(r)$. Solving systems (A6a)–(A6f) for $\{c_2^{\tau}\}$ leads to Eqs. (3.8a)–(3.8e). Note that expressions (A6a)–(A6c) are consistent with the tracelessness of $[Q]$, which is why the quadrupole tensor is completely described by the five (not six) independent quantities $c_2^{0,c}$, $c_2^{1,c}$, $c_2^{1,s}$, $c_2^{2,c}$, and $c_2^{2,s}$.

APPENDIX B: ANGULAR AVERAGING

We divide the r-axis into intervals $[0,\Delta[,[\Delta,2\Delta[,[2\Delta,3\Delta[,...,[(k-1)\Delta,k\Delta[,...$ and denote the middle of the kth interval by r_k $(k=1,2,3,\ldots)$. For every interval we define the quantity z_k,

$$z_k=\int_{(k-1)\Delta}^{k\Delta}r^2dr\int_0^{\pi}\sin\theta d\theta\int_0^{2\pi}d\phi\rho(\mathbf{r}). \tag{B1}$$

If factorization is assumed, z_k can be rewritten as

$$z_k=-et_kA, \tag{B2}$$

with

$$t_k=4\pi\int_{(k-1)\Delta}^{k\Delta}r^2dr\mathcal{R}(r), \tag{B3a}$$

$$A=\frac{1}{4\pi}\int_0^{\pi}\sin\theta d\theta\int_0^{2\pi}d\phi\mathcal{A}(\theta,\phi). \tag{B3b}$$

For sufficiently small intervals, t_k can be approximated by

$$t_k\approx 4\pi\Delta r_k^2\mathcal{R}(r_k). \tag{B4}$$

From Eqs. (B2) and (B4) we get

$$\mathcal{R}(r_k)\approx\frac{z_k}{-4\pi eAr_k^2\Delta}. \tag{B5}$$

Within the factorization assumption, it is natural to impose the normalization condition

$$4\pi\int_0^\infty r^2dr\mathcal{R}(r)=1, \tag{B6}$$

which implies $A=1$ since $\int d\mathbf{r}\rho(\mathbf{r})=-e$, so that

$$\mathcal{R}(r_k)\approx\frac{z_k}{-4\pi er_k^2\Delta}. \tag{B7}$$

[1] M. S. Dresselhaus, J. Dresselhaus, and P. C. Eklund, *Science of Fullerenes and Carbon Nanotubes* (Academic, New York, 1995).
[2] H. Kuzmany, B. Burger, and J. Kürti, in *Optical and Electronic Properties of Fullerenes and Fullerene-Based Materials*, edited by J. Shinar, Z. V. Vardeny, and Z. H. Kafafi (Dekker, New York, 2000).
[3] L. Forró and L. Mihály, Rep. Prog. Phys. **64**, 649 (2001).
[4] J. Winter and H. Kuzmany, Solid State Commun. **84**, 935 (1992); Q. Zhu, O. Zhou, J. E. Fischer, A. R. McGhie, W. J. Romanov, R. M. Strongin, M. A. Cichy, and A. B. Smith III, Phys. Rev. B **47**, 13948 (1993).
[5] O. Chauvet, G. Oszlányi, L. Forró, P. W. Stephens, M. Tegze, G. Faigel, and A. Jánossy, Phys. Rev. Lett. **72**, 2721 (1994).
[6] S. Pekker, L. Forró, L. Mihály, and A. Jánossy, Solid State Commun. **90**, 349 (1994).
[7] P. W. Stephens, G. Bortel, G. Faigel, M. Tegze, A. Jánossy, S. Pekker, G. Oszlányi, and L. Forró, Nature (London) **370**, 636 (1994).
[8] P. Launois, R. Moret, J. Hone, and A. Zettl, Phys. Rev. Lett. **81**, 4420 (1998); P. Launois, R. Moret, E. Llusca, J. Hone, and A. Zettl, Synth. Met. **103**, 2354 (1999).
[9] S. Rouzière, S. Margadonna, K. Prassides, and A. N. Fitch, Europhys. Lett. **51**, 314 (2000).
[10] A. M. Rao, P. Zhou, K.-A. Wang, G. T. Hager, J. M. Holden, Y. Wang, W.-T. Lee, X.-X. Bi, P. C. Eklund, and D. S. Cornett, Science **259**, 955 (1993).
[11] Y. Iwasa, T. Arima, R. M. Fleming *et al.*, Science **264**, 1570 (1994).
[12] I. O. Bashkin, V. I. Rashchupkin, A. F. Gurov, A. P. Moravsky, O. G. Rybchenko, N. P. Kobelev, Y. M. Soifer, and E. G. Ponyatovsky, J. Phys.: Condens. Matter **6**, 7491 (1994).
[13] M. Núñez-Regueiro, L. Marques, J. L. Hodeau, O. Béthoux, and M. Perroux, Phys. Rev. Lett. **74**, 278 (1995).
[14] C. S. Sundar, P. C. Sahu, V. S. Sastry *et al.*, Phys. Rev. B **53**, 8180 (1996).
[15] P.-A. Persson, U. Edlund, P. Jacobson, D. Johnels, A. Soldatov, and B. Sundqvist, Chem. Phys. Lett. **258**, 540 (1996).
[16] V. Agafonov, V. A. Davydov, L. S. Kashevarova, A. V. Rakhmanina, A. Kahn-Harari, P. Dubois, R. Céolin, and H. Szwarc, Chem. Phys. Lett. **267**, 193 (1997).
[17] R. Moret, P. Launois, P.-A. Persson, and B. Sundqvist, Europhys. Lett. **40**, 55 (1997).
[18] J. R. Fox, G. P. Lopinski, J. S. Lannin, G. B. Adams, J. B. Page, and J. E. Fischer, Chem. Phys. Lett. **249**, 195 (1996).
[19] H. M. Guerrero, R. L. Cappelletti, D. A. Neumann, and T. Yildirim, Chem. Phys. Lett. **297**, 165 (1998).
[20] A. Huq, P. W. Stephens, G. M. Bendele, and R. M. Ibberson, Chem. Phys. Lett. **347**, 13 (2001).
[21] K. H. Michel and A. V. Nikolaev, Phys. Rev. Lett. **85**, 3197 (2000).
[22] B. Verberck, K. H. Michel, and A. V. Nikolaev, J. Chem. Phys. **116**, 10462 (2002).
[23] A. V. Nikolaev and K. H. Michel, Solid State Commun. **117**, 739 (2001).
[24] K. H. Michel, B. Verberck, and A. V. Nikolaev (unpublished).
[25] B. Verberck, A. V. Nikolaev, and K. H. Michel, Phys. Rev. B **66**, 165425 (2002).
[26] D. Porezag, Th. Frauenheim, Th. Köhler, G. Seifert, and R. Kaschner, Phys. Rev. B **51**, 12947 (1995).
[27] W. I. F. David, R. M. Ibberson, J. C. Matthewman, K. Prassides, T. J. S. Dennis, J. P. Hare, H. W. Kroto, R. Taylor, and D. R. M. Walton, Nature (London) **353**, 147 (1991).
[28] C. J. Bradley and A. P. Cracknell, *The Mathematical Theory of Symmetry in Solids* (Clarendon, Oxford, 1972).
[29] A. V. Nikolaev and K. H. Michel, J. Chem. Phys. **117**, 4761 (2002).